THE JOURNAL OF PHYSICAL CHEMISTRY Letters

pubs.acs.org/JPCL Letter

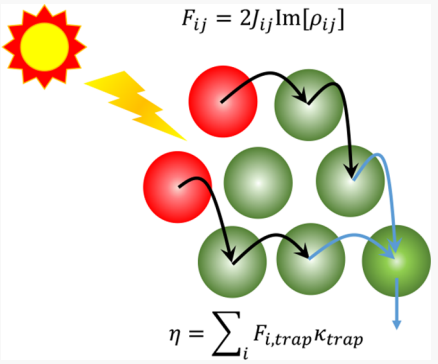
Steady-State Analysis of Light-Harvesting Energy Transfer Driven by Incoherent Light: From Dimers to Networks

Pei-Yun Yang and Jianshu Cao*

Cite This: J. Phys. Chem. Lett. 2020, 11, 7204−7211 Read Online

ACCESS | Metrics & More | Article Recommendations | Supporting Information

ABSTRACT: The question of how quantum coherence facilitates energy transfer has been intensively debated in the scientific community. Since natural and artificial light-harvesting units operate under the stationary condition, we address this question via a nonequilibrium steady-state analysis of a molecular dimer irradiated by incoherent sunlight and then generalize the key predictions to arbitrarily complex exciton networks. The central result of the steady-state analysis is the coherence−flux−efficiency relation: $\eta = c\sum_{i\neq j}F_{ij}\kappa_j = 2c\sum_{i\neq j}J_{ij}\mathrm{Im}[\rho_{ij}]\kappa_j$, where c is the normalization constant. In this relation, the first equality indicates that the energy transfer efficiency, η, is uniquely determined by the trapping flux, which is the product of the flux, F, and branching ratio, κ, for trapping at the reaction centers, and the second equality indicates that the energy transfer flux, F, is equivalent to the quantum coherence measured by the imaginary part of the off-diagonal density matrix, that is, $F_{ij} = 2J_{ij}\mathrm{Im}[\rho_{ij}]$. Consequently, maximal steady-state coherence gives rise to optimal efficiency. The coherence−flux−efficiency relation holds rigorously and generally for any exciton network of arbitrary connectivity under the stationary condition and is not limited to incoherent radiation or incoherent pumping. For light-harvesting systems under incoherent light, the nonequilibrium energy transfer flux (i.e., steady-state coherence) is driven by the breakdown of detailed balance and by the quantum interference of light excitations and leads to the optimization of energy transfer efficiency. It should be noted that the steady-state coherence or, equivalently, efficiency is the combined result of light-induced transient coherence, inhomogeneous depletion, and the system−bath correlation and is thus not necessarily correlated with quantum beatings. These findings are generally applicable to quantum networks and have implications for quantum optics and devices.

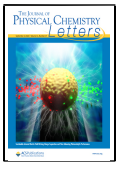


Ever since the first evidence of quantum coherence was demonstrated in photosynthetic systems, the role of quantum coherence in the light-harvesting process has inspired numerous scientific studies.[1,2] In particular, questions such as whether quantum coherence can be initiated by incoherent sunlight and whether coherence plays a role in the function of light-harvesting complexes have been extensively discussed in the literature.[3−11] Previous calculations[7] have shown that for the parameters relevant to photosynthetic systems, the exciton dynamics initiated by incoherent light exhibits dynamical coherence (quantum beatings) on the subpicosecond time scale; however, the transient coherent time scale may not be sufficiently long for the beatings to play a crucial role in efficient energy transfer to the reaction centers. Yet in natural systems, it is the nonequilibrium steady state (NESS) of the light-harvesting process that determines their functions, thus motivating the steady-state analysis reported here.

In addition to experimental relevance, our theoretical analysis is also inspired by previous studies of steady-state coherence in specific configurations of model systems.[12−14] In particular, it has been shown that nonvanishing steady-state coherence can enhance the efficiency of photosynthetic units and photovoltaic devices.[15−20] Despite these results, for molecular systems weakly driven by incoherent light, a general analytic theory is still lacking. More importantly, there is an urgent need for the community to elucidate how steady-state coherence relates to the detailed balance, energy transfer flux, optimal efficiency, and choice of basis set. In this work, we first address these open questions quantitatively using a light-driven dimer model and then extend to general quantum networks to reveal the crucial role of steady-state coherence in light-harvesting energy transfer.

To begin, we consider a generic molecular dimer illustrated in Figure 1a, which captures the essential physics relevant for the light-harvesting process. In particular, we adopt delocalized photon excitation and localized depletion but do not include delocalized radiative decay because it occurs on much slower time scale.[21] The case of delocalized trapping is analyzed in Section S5 of the Supporting Information and summarized later in the context of the "general dimer model". The

Received: May 27, 2020
Accepted: July 15, 2020
Published: August 6, 2020



Downloaded via MASSACHUSETTS INST OF TECHNOLOGY on September 9, 2020 at 18:10:56 (UTC).
See https://pubs.acs.org/sharingguidelines for options on how to legitimately share published articles.

ACS Publications © 2020 American Chemical Society

https://dx.doi.org/10.1021/acs.jpclett.0c01648
J. Phys. Chem. Lett. 2020, 11, 7204−7211

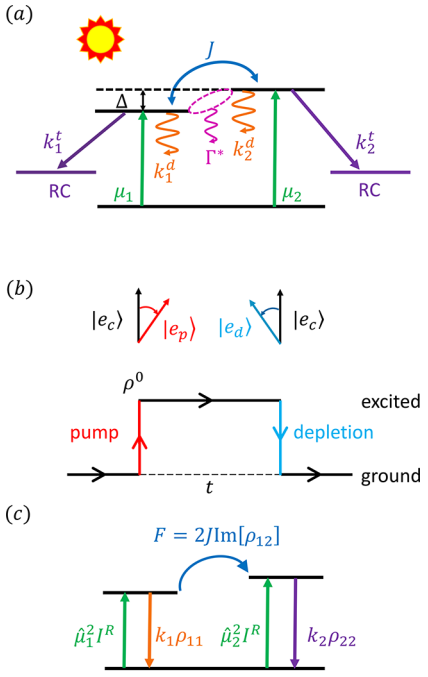


Figure 1. (a) Schematic of the dimer system consisting of two excited states with detuning Δ and a common ground state. The excited states are coupled to the intermolecular coupling, J. The depletion of the excited population of each molecule is quantified by $k_i = k_i^{\mathrm{t}} + k_i^{\mathrm{d}}$, where k_i^{t} characterizes the trapping to the reaction center and k_i^{d} characterizes the nonradiative irreversible decay to the ground state. Each molecule is further coupled to the local environment, leading to dephasing at a rate of Γ*. The nonequilibrium dynamics of the dimer system is driven by the interactions between the transition dipole moments of the dimer $\boldsymbol{\mu}_i$ and incoherent sunlight. (b) Schematic diagram for the rotations of the eigenstates by incoherent excitation (red line) and population depletion (blue line), where $|e_c\rangle$, $|e_p\rangle$, and $|e_d\rangle$ denote, respectively, the exciton states and eigenstates during the excitation and depletion processes. Note that the rotation of the eigenstates is proportional to $\boldsymbol{\mu}_+ \cdot \boldsymbol{\mu}_- = (\mu_1^2 - \mu_2^2)/2$ in the excitation process and proportional to $-\delta k$ in the depletion process. (c) Schematic of the steady-state population flux in the dimer system.

dynamics of the molecular dimer is dictated by the quantum master equation

$$\dot{\rho}(t) = -[L_{\mathrm{sys}} + L_{\mathrm{trap}} + L_{\mathrm{decay}} + L_{\mathrm{dissip}}]\rho(t) + \rho^0 \tag{1}$$

where the reduced Planck constant is set to unit $\hbar = 1$ hereafter. Here the Liouville superoperator $[L_{sys}]_{ij,kl} = i(H_{ik}\delta_{jl} - H_{lj}\delta_{ik})$ with $H_{ij} = (1 - \delta_{ij})J + \delta_{ij}\varepsilon_i$, where J is the intermolecular coupling and ε_i is the site energy of molecule i. In this Letter, we adopt the excitonic Hamiltonian and excitonic coherence, but the same treatment can apply to vibronic states and any other molecular states as well.[22] The population depletion of the dimer system originating from local energy trapping at the reaction center and irreversible decay to the ground state at each molecule is characterized by the Liouville superoperators $[L_{trap} + L_{decay}]_{ij,ij} = (k_i + k_j)/2$ with $k_i = k_i^{\mathrm{t}} + k_i^{\mathrm{d}}$, where k_i^{t} and k_i^{d} are the phenomenological trapping and decay rates at molecule i, respectively. The dissipation of the dimer due to the coupling to the environment is considered to be pure dephasing in the Haken−Strobl−Reineker (HSR) model,[23] where $[L_{\mathrm{dissip}}]_{ij,ij} = (1 - \delta_{ij})\Gamma^*$ with the pure dephasing rate Γ*. On the basis of the white noise approximation,[7] we have shown that the stationary incoherent sunlight induces a pure state given by

$$\rho^0 = [\rho_{11}^0, \rho_{12}^0, \rho_{21}^0, \rho_{22}^0] = I^R[\hat{\mu}_1^2, \hat{\boldsymbol{\mu}}_1 \cdot \hat{\boldsymbol{\mu}}_2, \hat{\boldsymbol{\mu}}_1 \cdot \hat{\boldsymbol{\mu}}_2, \hat{\mu}_2^2] \tag{2}$$

where $\hat{\boldsymbol{\mu}}_i = \boldsymbol{\mu}_i/\bar{\mu}$ is the normalized transition dipole, $\boldsymbol{\mu}_i$ is the transition dipole moment of molecule i, and $\bar{\mu} = \sqrt{\mu_1^2 + \mu_2^2}$ is the magnitude of the total dipole moment. The master eq 1 shows the generic interplay between the incoherent excitations and the population depletion and can reduce to the special cases discussed in the literature. (See Section S1B in the Supporting Information.)

Excitonic Coherence: Detailed Balance and Decomposition. The steady-state solution to eq 1 is derived and analyzed in Section S1 of the Supporting Information. For simplicity of presentation, we first consider the special case of the degenerate dimer ($\varepsilon_1 = \varepsilon_2 = \varepsilon$) without environmental effects ($\Gamma^* = 0$) and then extend our conclusions to the general dimer model. The NESS in the exciton basis is solved in the Supporting Information, giving

$$\rho_{++} = \frac{\hat{\mu}_+^2 I^R}{\bar{k}} + \frac{\delta k}{2J}\mathrm{Im}[\rho_{+-}] \tag{3a}$$

$$\rho_{--} = \frac{\hat{\mu}_-^2 I^R}{\bar{k}} + \frac{\delta k}{2J}\mathrm{Im}[\rho_{+-}] \tag{3b}$$

$$\rho_{+-} = -\frac{AI^R}{2}\frac{1 - i2J/\bar{k}}{(2J)^2 + k_1 k_2} \tag{3c}$$

where $\bar{k} = (k_1 + k_2)/2$ and $\delta k = (k_1 - k_2)/2$ and $\hat{\boldsymbol{\mu}}_\pm = (\hat{\boldsymbol{\mu}}_1 \pm \hat{\boldsymbol{\mu}}_2)/\sqrt{2}$ are defined on the exciton basis. A key prediction of the steady-state solution is the relationship between the exciton populations and the coherence. Specifically, the first terms in eqs 3a and 3b are the local contributions, which are the steady states for each exciton level without coherent mixing and are determined by the balance between the corresponding pumping and depletion rates. The second terms are the coherent mixing contributions, which are identical for both exciton states and are proportional to the imaginary part of quantum coherence $\mathrm{Im}[\rho_{+-}]$. Furthermore, the magnitude of the steady-state exciton coherence is proportional to $A \equiv \hat{\mu}_2^2 k_1 - \hat{\mu}_1^2 k_2$. The parameter A measures the deviation from the detailed balance

$$\frac{\hat{\mu}_1^2}{k_1} = \frac{\hat{\mu}_2^2}{k_2} \tag{4}$$

indicating a constant ratio of the excitation and depletion rates in the dimer. In some early analyses,[8] the light-harvesting system is coupled to a single thermal light source (e.g., blackbody radiation), where the detailed balance is automatically observed. Then, the coherence vanishes as the system relaxes to the thermal equilibrium. To break the detailed balance and induce steady-state coherence, light-harvesting systems must couple to at least another thermal bath, such as the protein environment or the reaction center, in addition to sunlight radiation.[7,14,17,24]

An equilibrium system weakly perturbed by thermal noise assumes the Boltzmann distribution in its eigenstates with zero exciton coherence. Therefore, the nonvanishing steady-state

https://dx.doi.org/10.1021/acs.jpclett.0c01648
J. Phys. Chem. Lett. 2020, 11, 7204−7211

exciton coherence arises from nonequilibrium driving, that is, the excitation by incoherent sunlight and the depletion from the excitation manifold. To quantify these two contributions, we decompose the NESS coherence in eq 3c into (see Section S2 in the Supporting Information)

$$\rho_{+-} = \rho_{+-}^{\text{light}} + \rho_{+-}^{\text{depletion}} = \left[\bar{k}\rho_{+-}^{0} - \frac{\delta k}{2}(\rho_{++}^{0} + \rho_{--}^{0})\right]\frac{1 - i2J/\bar{k}}{(2J)^2 + k_1 k_2} \tag{5}$$

where $\rho_{\pm\pm}^{0} = \hat{\mu}_{\pm}^2 I^R$ and $\rho_{+-}^{0} = (\hat{\boldsymbol{\mu}}_{+}\cdot\hat{\boldsymbol{\mu}}_{-})I^R$ are the light-induced initial state ρ^0 in eq 2 on the exciton basis. Thus the steady-state coherence can be induced by excitation and depletion, represented by the first and second terms in the brackets, respectively. Specifically, during the evolution of the light-harvesting dimer, its basis set rotates twice: The first rotation arises from the excitation process, where the incoherent radiation field creates the initial coherence ρ_{+-}^{0}, characterized by the effective transition dipole $\hat{\boldsymbol{\mu}}_{+}\cdot\hat{\boldsymbol{\mu}}_{-} = (\hat{\mu}_1^2 - \hat{\mu}_2^2)/2$, which is related to the quantum beatings previously discussed.[7] The second rotation occurs when the dimer system experiences asymmetric depletion ($\delta k \neq 0$) and is proportional to the initial population $\rho_{++}^{0} + \rho_{--}^{0}$. As shown in Figure 1b, the superposition of the two rotations is constructive when they are in phase, that is, $\delta\mu\delta k < 0$ ($\delta\mu = \mu_1 - \mu_2$), and is destructive when they are out of phase, $\delta\mu\delta k > 0$. An interesting finding from the previous analysis[7] is that light-induced transient coherence, as manifested as quantum beatings, relaxes on a time scale that is faster than the typical energy transfer time scale. However, eq 5 suggests that the exciton population can also contribute due to the asymmetry in population depletion, and thus the light-induced beatings may not dominate the steady-state coherence in photosynthetic systems.[7]

Intermolecular Coherence: Flux and Conservation Laws. To further explore the role of quantum coherence in light-harvesting energy transfer, we transform the steady-state solution in eq 3 to the local site basis (i.e., molecular basis), giving

$$\rho_{11} = \frac{\hat{\mu}_1^2 I^R}{k_1} - \frac{2J}{k_1}\text{Im}[\rho_{12}] = \frac{1}{k_1}(\rho_{11}^{0} - F) \tag{6a}$$

$$\rho_{22} = \frac{\hat{\mu}_2^2 I^R}{k_2} + \frac{2J}{k_2}\text{Im}[\rho_{12}] = \frac{1}{k_2}(\rho_{22}^{0} + F) \tag{6b}$$

$$\rho_{12} = \frac{I^R}{\bar{k}}\left(\hat{\boldsymbol{\mu}}_1\cdot\hat{\boldsymbol{\mu}}_2 - i\frac{AJ}{4J^2 + k_1 k_2}\right) \tag{6c}$$

In eqs 6a and 6b, the first terms are the incoherent monomer contributions, arising from the kinetic balance of the local excitation and the local population depletion in each molecule. The second terms are the coherent transfer contributions with opposite signs, indicating that the steady-state coherence induces a transfer flux between the two molecules of the dimer (see Figure 1c and Section S1A in the Supporting Information), that is

$$F = 2J\text{Im}[\rho_{12}] \propto A \tag{7}$$

The coherence–flux relation is completely general and was previously introduced[25] in the context of light-harvesting energy transfer and applied to Fenna–Matthews–Olson (FMO) and other model systems. Because of the local conservation of exciton population,[25] the transfer flux at any molecular site in a light-harvesting network is summed to zero. The second equality in eq 7 demonstrates that the deviation from the detailed balance, characterized by A, drives the nonequilibrium transfer between the two molecules via quantum coherence. Furthermore, we note that

$$\text{Im}[\rho_{12}] = -\text{Im}[\rho_{+-}] \tag{8}$$

such that the imaginary part of coherence is invariant to the choice of the basis set, which is an interesting observation given the recent discussion about the correct basis set to define quantum coherence in light-harvesting energy transfer.

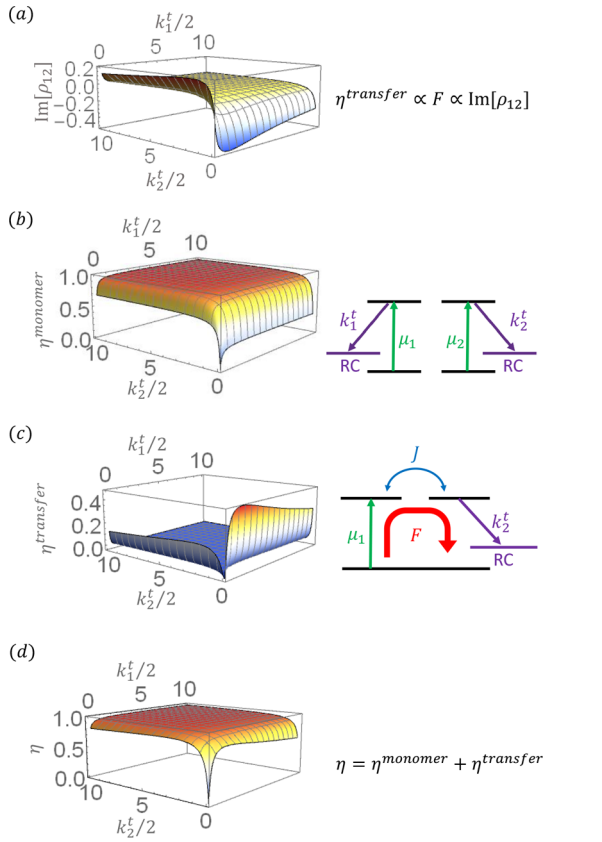


Figure 2. Quantum coherence and energy -transfer efficiency as a function of trapping rates k_i^t, with $J = 1$, $k^d = 0.25$, and $|\boldsymbol{\mu}_1|/|\boldsymbol{\mu}_2| = 2/3$: (a) $\text{Im}[\rho_{12}]$ in the unit of I^R, (b) monomer contribution, η^{monomer}, (c) transfer contribution, η^{transfer}, and (d) $\eta = \eta^{\text{monomer}} + \eta^{\text{transfer}}$.

In Figure 2a, we plot the NESS transfer flux as a function of the trapping rates k_1^t and k_2^t, assuming that the irreversible decay rates are the same for the dimer ($k_1^d = k_2^d = k^d$). The transfer flux is significant when either of the trapping rates is small and comparable to the decay rate, $k_i^t \approx k^d$, but vanishes when both trapping rates are large, that is, $k_1^t \gg k^d$ and $k_2^t \gg k^d$. When k_1^t (k_2^t) is smaller, the excitation flux flows from molecule 1 (2) to 2 (1), and the sign of the flux is positive (negative). Note that the magnitude of the flux is proportional to $\hat{\mu}_i^2$, which explains the asymmetry of the

https://dx.doi.org/10.1021/acs.jpclett.0c01648
J. Phys. Chem. Lett. 2020, 11, 7204–7211

diagram with $|\boldsymbol{\mu}_1| < |\boldsymbol{\mu}_2|$ in Figure 2. Later, it will be shown that the coherent part of efficiency η^{transfer} is proportional to F, thus explaining the similarity between Figure 2a and Figure 2c.

From the solution in eq 6, we obtain the NESS population flux in the dimer system, yielding

$$I^R = k_1\rho_{11} + k_2\rho_{22} \tag{9}$$

where I^R describes excitation by incoherent light, and the right-hand side describes the population depletion. As expected, these two fluxes are equal, as the exciton population is conserved in the steady-state limit. Interestingly, the excitation rate, I^R, is determined by the light intensity and the magnitudes of the transition dipoles, but it is independent of molecular configurations in light-harvesting complexes, such as the dipole orientation, intermolecular distance, and dipole−dipole interaction.

In the classical description, each molecule carries a fixed amount of excitation energy, so the energy flux is simply the product of the excitation energy and the exciton population flux, εI^R. This picture is modified in the presence of quantum coherence because the excitation energy is delocalized.[17] To see this quantitatively, we derive the excitation energy flux at the steady state (see Section S3 in the Supporting Information), giving

$$(\varepsilon + 2J\hat{\boldsymbol{\mu}}_1\cdot\hat{\boldsymbol{\mu}}_2)I^R = \varepsilon(k_1\rho_{11} + k_2\rho_{22}) + 2J\bar{k}\,\mathrm{Re}[\rho_{12}] \tag{10}$$

where the left and right-hand sides of the equation correspond to energy excitation and depletion, respectively, and are equal because of energy conservation. The first terms are exactly the classical result, $\varepsilon I^R = \varepsilon(k_1\rho_{11} + k_2\rho_{22})$, whereas the second terms are the quantum corrections, $2JI^R\hat{\boldsymbol{\mu}}_1\cdot\hat{\boldsymbol{\mu}}_2 = 2J\bar{k}\,\mathrm{Re}[\rho_{12}]$. Unlike the population flux, the quantum correction depends on the molecular configuration and is proportional to the real part of the coherence, $\mathrm{Re}[\rho_{12}]$. Thus, the real and imaginary parts of the quantum coherence have clear but different physical meanings in the energy transfer.

Optimal Efficiency. The excitation energy in light-harvesting systems can be trapped at the reaction center with a rate of k^{t} or dissipated via radiative or nonradiative channels with rate of k^{d}. Then, the efficiency of the light-harvesting energy transfer, η, can be defined as the trapping probability,[21,26−28] giving

$$\eta = \frac{\sum_i k_i^{\text{t}}\rho_{ii}}{\sum_i k_i^{\text{t}}\rho_{ii} + \sum_i k_i^{\text{d}}\rho_{ii}} = \frac{1}{I^R}\sum_i k_i^{\text{t}}\rho_{ii} \tag{11}$$

where the denominator is total exciton flux in eq 9, $\sum_i k_i^{\text{t}}\rho_{ii} + \sum_i k_i^{\text{d}}\rho_{ii} = I^R$. Inserting the steady-state density matrix in eq 6 into eq 11, we obtain

$$\eta = \eta^{\text{monomer}} + \eta^{\text{transfer}} = \sum_{i=1}^{2}\kappa_i\hat{\mu}_i^{\,2} - \frac{F}{I^R}(\kappa_1 - \kappa_2) \tag{12}$$

which consists of monomer and transfer contributions. Here $\kappa_i = k_i^{\text{t}}/k_i$ is the branching ratio for trapping at the ith site. For the monomer contribution, excitation and trapping occur locally at the same site, as shown schematically in Figure 2b, and the efficiency is the sum of local trapping probabilities. For the transfer contribution, the excitation is pumped at one site and transfers to the other site, as shown schematically in Figure 2c. In light-harvesting systems, light absorption and trapping usually occur on different molecules, so the efficiency is dominated by the transfer part, giving

$$\eta \propto F \propto \mathrm{Im}[\rho_{12}] \tag{13}$$

Thus the efficiency, η, is proportional to the exciton transfer flux, F, which, in turn, is determined by the quantum coherence, $\mathrm{Im}[\rho_{12}]$. Derived explicitly for the light-harvesting dimer, the coherence−flux−efficiency relation will be established later in eq 24 for arbitrary quantum networks.

In Figure 2, we plot η^{monomer} and η^{transfer} as a function of the trapping rates and can clearly identify two regimes. In the first regime (see Figure 2b), where both trapping rates are large, that is, $k_i^{\text{t}} \gg k^{\text{d}}$, the efficiency is dominated by the monomer contribution, η^{monomer}, as light absorption and energy trapping occur at the same molecule. When the two trapping rates are taken to be identical, $k_1^{\text{t}} = k_2^{\text{t}} \equiv k^{\text{t}}$, the energy transfer efficiency reduces to

$$\eta \simeq \frac{1}{1 + k^{\text{d}}\langle t\rangle} = \frac{1}{1 + k^{\text{d}}/k^{\text{t}}} \tag{14}$$

where the first equality is a general relation[21] that approximates the efficiency with the average trapping time, $\langle t\rangle$, and the second equality gives $\langle t\rangle = 1/k^{\text{t}}$ for this special case. Evidently, efficiency approaches 1 as k^{t} approaches infinity, so there is no nontrivial optimization for local transfer in the monomer regime.

In the second regime (see Figure 2c), where either of the trapping rates is small, that is, $k_i^{\text{t}} \le k^{\text{d}}$, the efficiency is dominated by the transfer contribution, η^{transfer}, and the excitation energy absorbed at one molecule is transferred to the reaction center at the other molecule. As observed in Figure 2c, in the transfer regime, there are apparent nontrivial optimal trapping rates for the maximal efficiency.[21,29−35] For example, with $k_1^{\text{t}} \approx k^{\text{d}}$, the average trapping time is given as (see Section S4 in Supporting Information)

$$\langle t\rangle = \frac{2}{k_2^{\text{t}}} + \hat{\mu}_1^{\,2}\frac{k_2^{\text{t}}}{4J^2} \tag{15}$$

which has a minimum as a function of k_2^{t}. In eq 15, $\hat{\mu}_1^{\,2}$ denotes the fraction of the delocalized excitation in the dimer. When $\hat{\mu}_1^{\,2} = 1$, the trapping time reduces to equation 4 in ref 21, an early result. Figure 2d plots the sum of the two contributions. Interestingly, the monomer and transfer regimes are complementary, so that the overall efficiency remains high over the entire parameter space, except in the small regime, where both trapping rates are small.

In the above, we have adopted a definition of energy transfer efficiency based on the exciton population flux, yet the analysis remains valid even when energy flux is used instead of population flux. On the basis of eq 10, we define efficiency in terms of the energy flow to the reaction center as

$$\eta_\epsilon = \frac{\varepsilon\eta + 2J\hat{\boldsymbol{\mu}}_1\cdot\hat{\boldsymbol{\mu}}_2\bar{\kappa}}{\varepsilon + 2J\hat{\boldsymbol{\mu}}_1\cdot\hat{\boldsymbol{\mu}}_2} \tag{16}$$

where $\bar{\kappa} = (\kappa_1 + \kappa_2)/2$. The first term in the numerator is exactly the site energy, ε, multiplied by the population transfer efficiency, η, defined in eq 11, which is the prediction of the classical picture, and the second term is the quantum correction, which is proportional to $\hat{\boldsymbol{\mu}}_1\cdot\hat{\boldsymbol{\mu}}_2$. In light-harvesting

https://dx.doi.org/10.1021/acs.jpclett.0c01648
J. Phys. Chem. Lett. 2020, 11, 7204−7211

systems, the site energy, ε, is much larger than the excitonic couplings, $\varepsilon \gg J$, so the second term is negligible, and we have $\eta_e \simeq \eta$.[36]

General Dimer Model. Although we have focused on the degenerate dimer model for simplicity, the solution presented in the Supporting Information is for the general dimer model, and the previously described analysis remains valid. Specifically, when the detuning $\varepsilon_2 - \varepsilon_1 = \Delta$ and the dephasing Γ^* are considered, the populations of the dimer remain the same as in eq 6, whereas the expression for quantum coherence is modified, giving

$$\mathrm{Im}[\rho_{12}] = -\mathrm{Im}[\rho_{+-}] = -I^R \frac{JA\Gamma - \Delta(\hat{\boldsymbol{\mu}}_1 \cdot \hat{\boldsymbol{\mu}}_2)k_1k_2}{4J^2\bar{k}\Gamma + (\Delta^2 + \Gamma^2)k_1k_2} \tag{17}$$

where $\Gamma = \Gamma^* + \bar{k}/2$. Clearly, in the presence of detuning, Δ, the quantum coherence also can be created by the interference of the transition dipole moments $\boldsymbol{\mu}_1 \cdot \boldsymbol{\mu}_2$ such that the detailed balance relation needs to be supplemented. Apart from this difference, our previous predictions including transfer flux, basis set invariance, decomposition, and flux conservation relations remain valid.

Because Δ and Γ^* appear only in the transfer contribution, η^{transfer}, we examine the energy transfer efficiency in the transfer regime. For convenience of analysis, we assume $k_1^{\mathrm{d}} = k_2^{\mathrm{d}} = k^{\mathrm{d}}$, $k_1^{\mathrm{t}} < k^{\mathrm{d}}$, and $k^{\mathrm{d}}/J \ll 1$ and obtain the average trapping time as

$$\langle t \rangle = \frac{2}{k_2^{\mathrm{t}}} + \hat{\mu}_1^{\,2}\frac{1}{2J^2}\frac{\Gamma^2 + \Delta^2}{\Gamma} - \hat{\boldsymbol{\mu}}_1 \cdot \hat{\boldsymbol{\mu}}_2 \frac{\Delta}{J\Gamma} \tag{18}$$

where the last two terms arise from quantum coherence. Equation 18 reduces to equation 4 in ref 21 when $\mu_2 = 0$, which exhibits a nontrivial optimal dephasing rate in the nondegenerate dimer ($\Delta \neq 0$). In the general case, in addition to the dephasing rate, the detuning and the transition dipoles also have nontrivial optimal conditions because of the interference, as given in the last term of eq 18. In Figure 3, the average trapping time in eq 18 is examined as a function of Δ and Γ^*, which shows a global optimal slightly away from the degenerate condition.

Before moving onto quantum networks, we briefly discuss the case of delocalized trapping by the introduction of the delocalized depletion rate, k_{12}. Then, the total exciton flux becomes

$$I^R = k_1\rho_{11} + k_2\rho_{22} + 2k_{12}\mathrm{Re}[\rho_{12}] \tag{19}$$

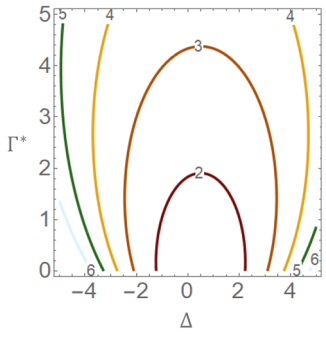


Figure 3. Contour of average trapping time as a function of detuning, $\Delta = \varepsilon_2 - \varepsilon_1$, and the dephasing rate, Γ^*. The model parameters are $J = 1$, $k_2^{\mathrm{t}} = 3$, $|\boldsymbol{\mu}_1|/|\boldsymbol{\mu}_2| = 2$, and $\boldsymbol{\mu}_1 // \boldsymbol{\mu}_2$.

where the exciton population created by incoherent excitation, I^R, decays through both localized and delocalized depletions. Following the steady-state solution in Section S5 of the Supporting Information, we obtain the formal expression for efficiency

$$\eta = \eta^{\mathrm{monomer}} + \eta^{\mathrm{transfer}} + \eta^{\mathrm{delocalized}} = \sum_{i=1,2} \kappa_i \hat{\mu}_i^{\,2} + \frac{1}{I^R}(\kappa_2 - \kappa_1)F + \frac{1}{I^R}(2 - \kappa_1 - \kappa_2)k_{12}^{\mathrm{t}}\mathrm{Re}[\rho_{12}] \tag{20}$$

which can be decomposed into monomer, transfer, and delocalized trapping contributions. Evidently, efficiency is correlated to both the real and imaginary parts of quantum coherence but with different physical meanings, consistent with a recent calculation reported in ref 37. The delocalized trapping is a simplified description of the generalized Förster energy transfer and super-radiance. A quantitative description of these collective processes requires the consideration of the system−bath correlation,[38] which is beyond the scope of this Letter.

Light-Harvesting Networks. It is straightforward to extend the master eq 1 to an arbitrary quantum network (see Figure 4),

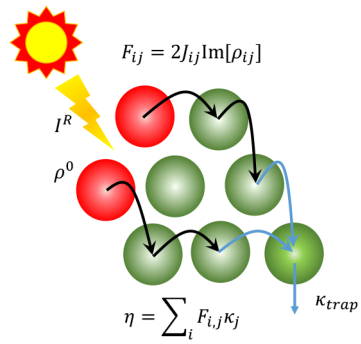


Figure 4. Schematic diagram of a light-harvesting network. The red molecules represent the chromophores excited by incoherent sunlight and the dark-green molecules represent the chromophores directly connected to the reaction center. The incoherent sunlight with intensity of I^R creates a stationary initial state ρ^0 under the white noise approximation. The excitation energy transfers through NESS flux between molecules $F_{ij} = 2J_{ij}\mathrm{Im}[\rho_{ij}]$ and finally is trapped at the reaction center with branching ratio κ_{trap}. Then, the energy transfer efficiency can be expressed as $\eta = c\sum_i F_{i,j}\kappa_j = c\sum_i F_{i,\mathrm{trap}}\kappa_{\mathrm{trap}}$, where $c = 1/I^R$ is the normalization constant.

that is, a multichromophoric system or a multilevel exciton system, with the excitonic coupling $J \to J_{ij}$ and the dephasing rate $\Gamma^* \to \Gamma_{ij}^*$. In the steady-state limit, the exciton population at site i is given in the form of (see Section S6 of the Supporting Information)

$$\rho_{ii} = \frac{1}{k_i}\left(\hat{\mu}_i^{\,2} I^R - \sum_{j \neq i} F_{ij}\right) \tag{21}$$

where the first term is the incoherent local contribution from monomers and the second term is the exciton transfer contribution characterized by the NESS flux between a pair of molecules

$$F_{ij} = 2J_{ij}\mathrm{Im}[\rho_{ij}] \tag{22}$$

https://dx.doi.org/10.1021/acs.jpclett.0c01648
J. Phys. Chem. Lett. 2020, 11, 7204−7211

As previously shown in ref 39, the flux thus defined characterizes the energy transfer pathways in a nonequilibrium quantum network. (Also see Figure 4.) Because the population flux is in the same form as in eq 9, $I^R = \sum_i k_i \rho_{ii}$, the energy transfer efficiency is then given by

$$\eta = \sum_i \kappa_i \hat{\mu}_i^2 - \frac{1}{I^R}\sum_{i<j}(\kappa_i - \kappa_j)F_{ij} = \sum_i \kappa_i \hat{\mu}_i^2 + \frac{1}{I^R}\sum_{i\neq j} F_{ij}\kappa_j \tag{23}$$

where the identity $F_{ij} = -F_{ji}$ is used to arrive the last expression. This definition has an intuitive interpretation based on network kinetics: The first term is the branching probability resulting from the local excitation and depletion associated with monomers, whereas the second term is the sum of all trapping flux to the reaction center. Here the trapping flux is understood as the product of transfer flux, F, and the branching ratio, κ. As in eq 13 for dimers, we now formally establish the coherence−flux−efficiency relation

$$\eta = \frac{1}{I^R}\sum_{i\neq j} F_{ij}\kappa_j = \frac{2}{I^R}\sum_{i\neq j} J_{ij}\mathrm{Im}[\rho_{ij}]\kappa_j \tag{24}$$

where we assume that the excitation and trapping occur on difference molecules. Equation 24 generally holds for any exciton networks of arbitrary connectivity under the stationary conditions, which is not limited to incoherent radiation or incoherent pumping.

Discussion. Light-harvesting systems are composed of many pigments, proteins, reaction centers, and so on and are thus far more complex than the model systems studied here. Yet our basic coherence−flux−efficiency relation remains valid. For applications to light-harvesting systems, we now comment on realistic considerations:

(1) For simplicity, the environment is treated classically as white noise, which yields dephasing but not thermalization. Our previous studies via numerical simulations and polaron calculations have shown that a quantum thermal bath leads to stationary coherence as a result of the noncanonical thermal distribution due to the system−bath correlation.[7,38] Thus the steady-state coherence is the combined result of light-induced beatings, inhomogeneous depletion, and thermalization and is thus not necessarily correlated with quantum beatings in 2D spectra.[40,41] Therefore, efficient energy transfer does not necessarily require long-lived quantum beatings (i.e., light-induced transient coherence), which is consistent with recent experimental evidence in FMO.[42,43]

(2) For the dimer model, quantum coherence defined by the imaginary part of the density matrix is basis-set invariant. Beyond the dimer model, quantum coherence depends on the choice of basis set, thus raising the question of the right basis.[35] Yet physical measurements are independent of the choice of basis, so this question is for the convenience of theoretical description and numerical approximation. Typically, the local basis is a natural choice for describing transport, whereas the exciton basis is more convenient for calculating spectroscopy. Because light-harvesting systems are strongly coupled to the protein environment, the polaron basis provides a physically motivated description.[13]

(3) The flux−coherence relation can be defined between any pairs of molecules, $F_{ij} = 2J_{ij}\mathrm{Im}[\rho_{ij}]$, and is shown to be general in appendix B of ref 25. Interestingly, this relation reduces to the classical flux in the strong damping limit, $F_{ij} = \rho_i k_{ij} - \rho_j k_{ji}$, where k is the hopping rate (e.g., Förster rate for energy transfer). This classical limit is the leading term of a systematic mapping of quantum networks to kinetic networks,[39] which allows a perturbative calculation of long-range transfer.[44] In FMO, the parametric dependence of the energy transfer efficiency can be reproduced by the classical flux, suggesting the dominance of the hopping mechanism.[25] Yet regardless of stepwise hopping or wave-like propagation, the coherence−flux−efficiency relation holds rigorously and generally.

(4) In photosynthetic systems, the number of light-absorption pigments is larger than the number of reaction centers, so that the excitation energy funnels to the reaction centers driven by energetic and entropic gradients.[45,46] In this case, light-harvesting systems can be optimized for their functions, not only via coherence but also via composition and spatial arrangements. The optimization of self-assembly superstructures has been studied in purple bacteria membranes as an illustrative example of light-harvesting networks.[47,48]

In summary, we have demonstrated that steady-state coherence leads to optimal energy transfer in light-harvesting systems. Specifically, as given explicitly in eq 24, the efficiency, η, is proportional to the exciton transfer flux, F, which, in turn, is determined by the quantum coherence $\mathrm{Im}[\rho]$. The coherence−flux−efficiency relation holds rigorously and generally for any exciton network of arbitrary connectivity under the stationary conditions, which is not limited to incoherent radiation or incoherent pumping. For light-harvesting networks under incoherent sunlight, the nonequilibrium energy transfer flux is driven by the breakdown of the detailed balance and by the quantum interference of light excitations. It should be noted that the steady-state coherence or, equivalently, the energy transfer flux is the combined result of light-induced transient coherence, inhomogeneous depletion, and system−bath correlation and is thus not necessarily correlated with quantum beatings in 2D spectra. These findings reveal the crucial role of steady-state quantum coherence in light-harvesting systems and have implications for quantum biology and quantum optics.

■ ASSOCIATED CONTENT

Supporting Information

The Supporting Information is available free of charge at https://pubs.acs.org/doi/10.1021/acs.jpclett.0c01648.

S1. Master equation and steady-state solution. S2. Decomposition of steady-state coherence. S3. Energy flux. S4. Average trapping time. S5. Delocalized trapping. S6. Quantum networks (PDF)

■ AUTHOR INFORMATION

Corresponding Author

Jianshu Cao − *Department of Chemistry, Massachusetts Institute of Technology, Cambridge, Massachusetts 02139, United States*; orcid.org/0000-0001-7616-7809; Email: jianshu@mit.edu

Author

Pei-Yun Yang − *Department of Chemistry, Massachusetts Institute of Technology, Cambridge, Massachusetts 02139, United States*

Complete contact information is available at: https://pubs.acs.org/10.1021/acs.jpclett.0c01648

https://dx.doi.org/10.1021/acs.jpclett.0c01648
J. Phys. Chem. Lett. 2020, 11, 7204−7211

Notes

The authors declare no competing financial interest.

■ ACKNOWLEDGMENTS

This work is supported by the NSF (CHE 1800301 and CHE 1836913). P.-Y.Y. was partially supported by the Ministry of Science and Technology overseas project of Taiwan under grant ID number 107-2917-I-564-011. The key results of this paper were presented at the Banff meeting, August 2019. We thank Prof. Paul Brumer for the helpful discussions and for the exchange of recent manuscripts.

■ REFERENCES

(1) Scholes, G. D.; Fleming, G. R.; Chen, L. X.; Aspuru-Guzik, A.; Buchleitner, A.; Coker, D. F.; Engel, G. S.; Van Grondelle, R.; Ishizaki, A.; Jonas, D. M.; et al. Using Coherence to Enhance Function in Chemical and Biophysical Systems. *Nature* **2017**, *543*, 647−656.

(2) Cao, J.; Cogdell, R. J.; Coker, D. F.; Duan, H.-G.; Hauer, J.; Kleinekathöfer, U.; Jansen, T. L. C.; Mančal, T.; Miller, R. J. D.; Ogilvie, J. P.; et al. Quantum biology revisited. *Sci. Adv.* **2020**, *6*, No. eaaz4888.

(3) Cheng, Y.-C.; Fleming, G. R. Dynamics of light harvesting in photosynthesis. *Annu. Rev. Phys. Chem.* **2009**, *60*, 241−262.

(4) Mančal, T.; Valkunas, L. Exciton dynamics in photosynthetic complexes: excitation by coherent and incoherent light. *New J. Phys.* **2010**, *12*, 065044.

(5) Ishizaki, A.; Fleming, G. R. Quantum coherence in photosynthetic light harvesting. *Annu. Rev. Condens. Matter Phys.* **2012**, *3*, 333−361.

(6) Turner, D. B.; Arpin, P. C.; McClure, S. D.; Ulness, D. J.; Scholes, G. D. Coherent multidimensional optical spectra measured using incoherent light. *Nat. Commun.* **2013**, *4*, 2298.

(7) Olšina, J.; Dijkstra, A. G.; Wang, C.; Cao, J. Can Natural Sunlight Induce Coherent Exciton Dynamics? 2014, arXiv:1408.5385. arXiv.org e-Print archive. https://arxiv.org/abs/1408.5385.

(8) Tscherbul, T. V.; Brumer, P. Long-lived quasi-stationary coherences in a v-type system driven by incoherent light. *Phys. Rev. Lett.* **2014**, *113*, 113601.

(9) Brumer, P. Shedding (Incoherent) Light on Quantum Effects in Light-Induced Biological Processes. *J. Phys. Chem. Lett.* **2018**, *9*, 2946−2955.

(10) Shatokhin, V. N.; Walschaers, M.; Schlawin, F.; Buchleitner, A. Coherence turned on by incoherent light. *New J. Phys.* **2018**, *20*, 113040.

(11) Chan, H. C.; Gamel, O. E.; Fleming, G. R.; Whaley, K. B. Single-photon absorption by single photosynthetic light-harvesting complexes. *J. Phys. B: At., Mol. Opt. Phys.* **2018**, *51*, 054002.

(12) Kozlov, V. V.; Rostovtsev, Y.; Scully, M. O. Inducing quantum coherence via decays and incoherent pumping with application to population trapping, lasing without inversion, and quenching of spontaneous emission. *Phys. Rev. A: At., Mol., Opt. Phys.* **2006**, *74*, 063829.

(13) Xu, D.; Cao, J. Non-canonical distribution and non-equilibrium transport beyond weak system-bath coupling regime: A polaron transformation approach. *Front. Phys.* **2016**, *11*, 110308.

(14) Tscherbul, T. V.; Brumer, P. Non-equilibrium stationary coherences in photosynthetic energy transfer under weak-field incoherent illumination. *J. Chem. Phys.* **2018**, *148*, 124114.

(15) Scully, M. O.; Chapin, K. R.; Dorfman, K. E.; Kim, M. B.; Svidzinsky, A. Quantum heat engine power can be increased by noise-induced coherence. *Proc. Natl. Acad. Sci. U. S. A.* **2011**, *108*, 15097−15100.

(16) Dorfman, K. E.; Voronine, D. V.; Mukamel, S.; Scully, M. O. Photosynthetic reaction center as a quantum heat engine. *Proc. Natl. Acad. Sci. U. S. A.* **2013**, *110*, 2746−2751.

(17) Xu, D.; Wang, C.; Zhao, Y.; Cao, J. Polaron effects on the performance of light-harvesting systems: a quantum heat engine perspective. *New J. Phys.* **2016**, *18*, 023003.

(18) Dorfman, K. E.; Xu, D.; Cao, J. Efficiency at maximum power of a laser quantum heat engine enhanced by noise-induced coherence. *Phys. Rev. E: Stat. Phys., Plasmas, Fluids, Relat. Interdiscip. Top.* **2018**, *97*, 042120.

(19) Zhang, Y.; Oh, S.; Alharbi, F. H.; Engel, G. S.; Kais, S. Delocalized quantum states enhance photocell efficiency. *Phys. Chem. Chem. Phys.* **2015**, *17*, 5743−5750.

(20) Rouse, D. M.; Gauger, E. M.; Lovett, B. W. Optimal Power Generation Using Dark States in Dimers Strongly Coupled to Their Environment. *New J. Phys.* **2019**, *21*, 063025.

(21) Cao, J.; Silbey, R. J. Optimization of exciton trapping in energy transfer processes. *J. Phys. Chem. A* **2009**, *113*, 13825−13838.

(22) The molecular origin of "quantum beats" in 2D spectroscopy has been debated in literature but is beyond the scope of this Letter. The readers can find discussions in recent reviews. In this Letter, we use excitonic coherence and the Hamiltonian for the convenience of presentation, but the basic concept and analysis can be applied to any quantum state.

(23) Haken, H.; Reineker, P. The coupled coherent and incoherent motion of excitons and its influence on the line shape of optical absorption. *Eur. Phys. J. A* **1972**, *249*, 253−268.

(24) Koyu, S.; Dodin, A.; Brumer, P.; Tscherbul, T. V. Steady-State Fano Coherences in a V-type System Driven by Polarized Incoherent Light. 2020, arXiv:2001.09230. arXiv.org e-Print archive. https://arxiv.org/abs/2001.09230.

(25) Wu, J.; Liu, F.; Ma, J.; Silbey, R. J.; Cao, J. Efficient energy transfer in light-harvesting systems II: Quantum-classical comparison, flux network, and robustness analysis. *J. Chem. Phys.* **2012**, *137*, 174111.

(26) Rebentrost, P.; Mohseni, M.; Kassal, I.; Lloyd, S.; Aspuru-Guzik, A. Environment-assisted quantum transport. *New J. Phys.* **2009**, *11*, 033003.

(27) Chin, A. W.; Datta, A.; Caruso, F.; Huelga, S. F.; Plenio, M. B. Noise-assisted energy transfer in quantum networks and light-harvesting complexes. *New J. Phys.* **2010**, *12*, 065002.

(28) Wu, J.; Liu, F.; Shen, Y.; Cao, J.; Silbey, R. J. Efficient energy transfer in light-harvesting systems, I: Optimal temperature, reorganization energy and spatial-temporal correlations. *New J. Phys.* **2010**, *12*, 105012.

(29) Wu, J.; Silbey, R. J.; Cao, J. Generic mechanism of optimal energy transfer efficiency: A scaling theory of the mean first-passage time in exciton systems. *Phys. Rev. Lett.* **2013**, *110*, 200402.

(30) Jesenko, S.; Žnidarič, M. Excitation Energy Transfer Efficiency: Equivalence of Transient and Stationary Setting and the Absence of Non-Markovian Effects. *J. Chem. Phys.* **2013**, *138*, 174103.

(31) Leon-Montiel, R.; Kassal, I.; Torres, J. Importance of excitation and trapping conditions in photosynthetic environment-assisted energy transport. *J. Phys. Chem. B* **2014**, *118*, 10588.

(32) Zhang, Y.; Celardo, G.; Borgonovi, F.; Kaplan, L. Opening-assisted coherent transport in the semiclassical regime. *Phys. Rev. E: Stat. Phys., Plasmas, Fluids, Relat. Interdiscip. Top.* **2017**, *95*, 022122.

(33) Zerah-Harush, E.; Dubi, Y. Universal Origin for Environment-Assisted Quantum Transport in Exciton Transfer Networks. *J. Phys. Chem. Lett.* **2018**, *9*, 1689−1695.

(34) Dutta, R.; Bagchi, B. Quantum Coherence and Its Signatures in Extended Quantum Systems. *J. Phys. Chem. B* **2020**, *124*, 4551.

(35) Tomasi, S.; Kassal, I. Classification of coherent enhancements of light-harvesting processes. *J. Phys. Chem. Lett.* **2020**, *11*, 2348−2355.

(36) Manzano, D. Quantum transport in networks and photosynthetic complexes at the steady state. *PLoS One* **2013**, *8*, No. e57041.

(37) Jung, K. A.; Brumer, P. Energy Transfer under Natural Incoherent Light: Effects of Asymmetry on Efficiency. 2020, arXiv:2007.00783. arXiv.org e-Print archive. https://arxiv.org/abs/2007.00783.

(38) Ma, J.; Cao, J. Förster resonance energy transfer, absorption and emission spectra in multichromophoric systems. I. Full cumulant

https://dx.doi.org/10.1021/acs.jpclett.0c01648
J. Phys. Chem. Lett. 2020, 11, 7204−7211

expansions and system-bath entanglement. *J. Chem. Phys.* **2015**, *142*, 094106.
(39) Wu, J.; Cao, J. Higher-order kinetic expansion of quantum dissipative dynamics: Mapping quantum networks to kinetic networks. *J. Chem. Phys.* **2013**, *139*, 044102.
(40) Engel, G. S.; Calhoun, T. R.; Read, E. L.; Ahn, T.-K.; Mančal, T.; Cheng, Y.-C.; Blankenship, R. E.; Fleming, G. R. Evidence for wavelike energy transfer through quantum coherence in photosynthetic systems. *Nature* **2007**, *446*, 782−786.
(41) Collini, E.; Wong, C. Y.; Wilk, K. E.; Curmi, P. M. G.; Brumer, P.; Scholes, G. D. Coherently wired light-harvesting in photosynthetic marine algae at ambient temperature. *Nature* **2010**, *463*, 644−647.
(42) Duan, H.-G.; Prokhorenko, V. I.; Cogdell, R. J.; Ashraf, K.; Stevens, A. L.; Thorwart, M.; Miller, R. J. D. Nature does not rely on long-lived electronic quantum coherence for photosynthetic energy transfer. *Proc. Natl. Acad. Sci. U. S. A.* **2017**, *114*, 8493−8498.
(43) Thyrhaug, E.; Tempelaar, R.; Alcocer, M. J. P.; Žídek, K.; Bína, D.; Knoester, J.; Jansen, L.; Zigmantas, D. Identification and characterization of diverse coherences in the Fenna-Matthews-Olson complex. *Nat. Chem.* **2018**, *10*, 780−786.
(44) Skourtis, S.; Mukamel, S. Superexchange versus sequential long range electron transfer; density matrix pathways in Liouville space. *Chem. Phys.* **1995**, *197*, 367.
(45) Moix, J.; Wu, J.; Huo, P.; Coker, D.; Cao, J. Efficient energy transfer in light-harvesting systems, III: The influence of the eighth bacteriochlorophyll on the dynamics and efficiency in FMO. *J. Phys. Chem. Lett.* **2011**, *2*, 3045−3052.
(46) Adolphs, J.; Renger, T. How proteins trigger excitation energy transfer in the FMO complex of green sulfur bacteria. *Biophys. J.* **2006**, *91*, 2778−2797.
(47) Hu, X.; Damjanović, A.; Ritz, T.; Schulten, K. Architecture and mechanism of the light-harvesting apparatus of purple bacteria. *Proc. Natl. Acad. Sci. U. S. A.* **1998**, *95*, 5935−5941.
(48) Cleary, L.; Chen, H.; Chuang, C.; Silbey, R. J.; Cao, J. Optimal fold symmetry of LH2 rings on a photosynthetic membrane. *Proc. Natl. Acad. Sci. U. S. A.* **2013**, *110*, 8537−8542.

https://dx.doi.org/10.1021/acs.jpclett.0c01648
J. Phys. Chem. Lett. 2020, 11, 7204−7211